Published in final edited form as:
Neuron. 2007 September 6; 55(5): 799–808. doi:10.1016/j.neuron.2007.07.037.

Specialized Circuits from Primary Visual Cortex to V2 and Area MT

Jonathan J. Nassi and **Edward M. Callaway**
Systems Neurobiology Laboratories, The Salk Institute for Biological Studies, 10010 North Torrey Pines Road, La Jolla, CA 92037, U.S.A

Abstract

Primary visual cortex (V1) integrates inputs from parallel magnocellular (M) and parvocellular (P) streams and recombines them to create functionally specialized outputs. Numerous studies have demonstrated the role of columnar or laminar compartments in this process. However, a clear understanding of the relationships between inputs and outputs is complicated by the fact that layer 4B, which provides outputs to dorsal visual areas, contains multiple cell types with the potential to be uniquely connected. Using a modified rabies virus that expresses green fluorescent protein, we show that layer 4B neurons projecting to MT are a majority spiny stellate, whereas those projecting to V2 are overwhelmingly pyramidal. Regardless of cell type, neurons projecting to MT have larger cell bodies, more total dendritic length, and are located deeper within layer 4B. Furthermore, pyramidal neurons projecting to MT are located preferentially underneath cytochrome oxidase blobs, indicating that MT-projecting neurons of both types restrict their dendrites to M-recipient zones. We conclude that MT-projecting layer 4B neurons are specialized for the fast transmission of information from the M pathway, while V2-projecting neurons are likely to mediate slower computations involving mixed M and P signals.

In the primate visual system, sensory input is parsed into magnocellular (M), parvocellular (P), and koniocellular (K) processing streams and relayed from the retina to primary visual cortex (V1) along routes which are anatomically separate and distinct (Blasdel and Lund, 1983; Dacey, 2000; Hendrickson et al., 1978; Hendry and Reid, 2000; Hendry and Yoshioka, 1994; Michael, 1988). Within V1, the anatomical circuitry quickly becomes more complex, with substantial convergence of M, P, and K pathways (Lachica et al., 1992; Yabuta and Callaway, 1998; Yabuta et al., 2001; Yoshioka et al., 1994). The mixing of early parallel pathways within V1 and the apparent lack of compartmentalization in outputs from V1 to extrastriate cortical areas (Sincich and Horton, 2002; Xiao and Felleman, 2004), has been used as evidence for non-specificity within cortex and has led some to reject parallel processing models of the primate visual system. Nevertheless, the striking cell type specificity of local connection patterns within V1 (Callaway, 1998a) leaves open the possibility that outputs from V1 to extrastriate cortical areas relay specialized circuits with specific combinations of early parallel pathway input.

Beyond V1, visual information is processed in relatively independent dorsal and ventral streams (DeYoe and Van Essen, 1988; Livingstone and Hubel, 1988; Merigan and Maunsell, 1993; Zeki and Shipp, 1988). Dorsal stream cortical areas are specialized for analyses of object motion and spatial relationships, and ventral stream cortical areas are specialized for analyses of object attributes such as shape and color (Desimone and Ungerleider, 1989). Dorsal stream

cortical areas receive their strongest input from layer 4B of V1, which connects directly with MT, V3, and the cytochrome oxidase (CO) thick stripes of V2 (Burkhalter et al., 1986; Livingstone and Hubel, 1987; Shipp and Zeki, 1989). It was long thought that layer 4B received input only from the M pathway through layer 4Cα, sending an M-dominated signal to dorsal stream cortical areas. However, in more recent years, photostimulation studies on monkey V1 slices showed that pyramidal cells in layer 4B of V1 receive functional input from both M-dominated layer 4Cα and P-dominated layer 4Cβ (Yabuta et al., 2001). While pyramidal cells make up the majority cell type within layer 4B (Callaway and Wiser, 1996), a minority of cells have spiny stellate morphology and receive input only from M-dominated layer 4Cα, suggesting a possible means by which the dorsal stream could receive an M-dominated signal (Yabuta et al., 2001).

The projection from layer 4B of V1 to MT has been studied extensively in different primate species and using different methodological approaches (Boyd and Casagrande, 1999; Elston and Rosa, 1997; Shipp and Zeki, 1989; Tigges et al., 1981; vogt Weisenhorn et al., 1995). While available evidence suggests that MT in macaque monkey receives input from both spiny stellate and pyramidal cells in layer 4B of V1 (Shipp and Zeki, 1989; Sincich and Horton, 2003), attempts to definitively identify and quantify the proportions of each cell type have been limited due to technical considerations including partial cell fills and tangential sectioning. Although it is known that the neurons in layer 4B that project to MT are a separate population from those projecting to V2 (Sincich and Horton, 2003), it is unclear how these two populations differ morphologically. In the present study, we use a rabies virus that has been modified to serve as a powerful monosynaptic retrograde tracer by replacing the virus glycoprotein with green fluorescent protein (GFP) in its genome (Wickersham et al., 2007). By injecting this rabies virus into MT or V2, we obtained detailed dendritic morphology and were able to make quantitative comparisons between the cells projecting from layer 4B of V1 to these extrastriate cortical areas. We find that cells projecting to MT are a majority spiny stellate, whereas those projecting to V2 are overwhelmingly pyramidal. Morphological differences such as cell body size and total dendritic length further differentiate the two cell populations regardless of cell type. Finally, differences exist in the tangential distribution of these populations relative to the overlying pattern of CO blobs and interblobs, with pyramidal cells projecting to MT biased toward blobs. Thus, both spiny stellate and pyramidal neurons that project from V1 to MT restrict their dendrites to locations that receive input from M-recipient layer 4Cα. These results provide evidence for specialized and distinct circuits in V1 that relay a fast M-dominated signal to MT and a mixed M and P signal to V2.

RESULTS

We used a modified, GFP-expressing rabies virus as a monosynaptic retrograde tracer to study connections from V1 to areas MT and V2 of macaque monkey (Wickersham et al., 2007). In particular, we were interested in determining the proportion of pyramidal versus spiny stellate cells in layer 4B of V1 that project directly to MT or V2. Injections of rabies virus were targeted to cortical area MT of two macaque monkeys (three hemispheres) and V2 of two macaque monkeys (two hemispheres) (see Experimental Procedures). After a 7 day survival period (3 day survival period for JNM2) the animals were perfused, and the brains were sectioned and stained for CO and an antibody against GFP (see Experimental Procedures). The locations of the injections were confirmed histologically to be confined to either MT (Figures 1A–B) or V2 (Figure 1C) (see Experimental Procedures). The injected rabies virus infected glial cells at the injection site, allowing visualization of the needle track in sections stained for GFP. For MT cases, adjacent sections stained for myelin or Nissl were used to confirm that the needle penetration passed within the region of dense and uniform myelination along the posterior bank of the superior temporal sulcus (STS) typical of MT (Figures 1A–B). In V2 cases, the needle penetrations could be seen anterior to the distinctive CO pattern of V1 (Figure 1C). Upon

examining histological sections, retrogradely labeled cells were found in visual areas known to have monosynaptic connections with the cortical area injected. As expected, extrastriate cortical areas that are known to provide feedforward input to MT had labeled cells confined to supragranular layers, and areas known to provide feedback input to MT or V2 had labeled cells confined to infragranular layers (Maunsell and van Essen, 1983).

Following MT injections, labeled cells within V1 were found in layers 4B and 6 as expected from previous reports (Figures 2A–B) (Shipp and Zeki, 1989). Labeled cells were scattered in the calcarine sulcus (JNM2, JNM14) and on the opercular surface (JNM14). The total number and density of rabies/GFP labeled cells, however, were lower than observed with standard tracers (Table 1), likely due to technical considerations such as rabies virus titer and efficiency of viral uptake at axons terminals. The number of layer 6 Meynert cells labeled in these cases was approximately 1 for every 10 layer 4B cells and were not numerous enough to analyze further (data not shown). The number of cells labeled in layer 4B, however, was substantial (Figures 2A–B). GFP was expressed throughout each cell's processes, allowing for extensive morphological analysis (Figures 2A–B and 3A). In fact, classifying layer 4B cells as either pyramidal or spiny stellate was quite straightforward. Averaged across cases, 76% of layer 4B cells retrogradely labeled from MT injections were of spiny stellate morphology, with the remaining 24% pyramidal (Table 1; Figure 3C). There was some variation between cases, with as high as 93% spiny stellate cells in JNM2 and as low as 67% spiny stellate cells in JNM14L. This variation was not an obvious result of eccentricity, and may more likely be a result of variation at the MT injection site (i.e. different laminar depths). Nevertheless, in all cases the population of retrogradely labeled cells in layer 4B was at least two thirds spiny stellate (Figure 3C). It has been estimated previously by blind intracellular fills of layer 4B neurons in macaque V1 slice that pyramidal cells make up an approximate two thirds majority (Callaway and Wiser, 1996). The proportion of spiny stellates we observed after MT injections, therefore, was significantly higher than expected from a random sampling of layer 4B cells (Fisher's exact test, $p < 0.05$).

Following V2 injections, labeled cells within V1 were found in all layers outside of layer 4C. Particularly large numbers of labeled cells were found in layer 2/3 (data not shown), with substantial numbers of rabies/GFP labeled cells in layer 4B (Table 1; Figure 2C). We did not localize our V2 injections to particular stripe types and likely injected into multiple stripe types with each penetration. There is some indication that layer 4B projects to pale stripes in addition to thick stripes in V2 (Sincich and Horton, 2002), however it remains likely that the majority of the layer 4B cells retrogradely labeled are the result of injections including a thick stripe in V2 (Sincich et al., 2007). Striking morphological detail was again obtained, allowing for rather straightforward classification of cells as either pyramidal or spiny stellate (Figures 2C and 3B). Averaged across cases, 83% of layer 4B cells retrogradely labeled from V2 injections were of pyramidal morphology, with the remaining 17% spiny stellate (Table 1;Figure 3C). There was little variation between the two cases, with 85% pyramidal cells in JNM8 and 82% pyramidal cells in JNM12. The proportion of pyramids we observed following V2 injections was not statistically different from that expected from a random sampling of layer 4B cells (Fisher's exact test, $p > 0.05$) (Callaway and Wiser, 1996). In striking contrast, the proportion of cell types projecting from layer 4B of V1 to MT is overwhelming spiny stellate and significantly different from the proportion of cell types projecting to V2 (Fisher's exact test, $p < 0.001$) (Figure 3C). These results suggest highly specialized circuits relaying different visual information to MT or V2.

While the populations of cells projecting from layer 4B of V1 to MT or V2 have very different cell type proportions, they nevertheless include both cell types in substantial number. We were, therefore, interested to investigate whether additional differences exist between the two cell populations. It has been reported previously that the two populations differ in cell body size

(Sincich and Horton, 2003), and we indeed confirmed this finding (Table 2; Figure 4A). On average, cell bodies of MT-projecting cells were more than double the size of V2-projecting cells (MT: 329μm^2, V2: 146μm^2; t-test, $p < 0.001$). Cell body size did not depend on cell type, as there was no significant difference between pyramids and stellates for a given cortical injection target (Table 2; Figure 4A). The distributions of cell body sizes do overlap substantially, however, with the largest V2-projecting cells having similar sizes to the smallest MT-projecting cells (Figure 4A). V2-projecting cells were also found to be located more superficially in layer 4B (laminar depth index = 0.68) than MT-projecting cells (laminar depth index = 0.78) (Mann-Whitney test, $p < 0.02$) (Table 2; Figure 4B). While stellates projecting to V2 are consistently found toward the very bottom of layer 4B (laminar depth index = 0.90), pyramids projecting to V2 are found more superficially and throughout the layer (laminar depth index = 0.63) (Mann-Whitney test, $p < 0.001$). It is likely that the deeper locations of the MT-projecting cells allow them to receive substantial input from within layer 4Cα.

In order to further assess more subtle differences in the two cell populations, we fully reconstructed the dendrites of a subset of cells projecting either to MT (5 stellate, 5 pyramidal) or V2 (3 stellate, 5 pyramidal) (Figures 3A–B). As expected, both pyramids and spiny stellates projecting to MT or V2 had the majority of their dendritic length in layer 4B (approximately 70%) (Table 3). Somewhat surprising, however, was the high percentage of dendritic length (approximately 20%) in layer 4Cα and the small percentage of dendritic length consistently present in layer 4A (approximately 2%). Dendrites were never found to extend below layer 4Cα and only the apical dendrites of pyramidal cells extended above layer 4A (Table 3; Figures 3A–B). These apical dendrites were typically non-tufted (approximately 75%) and of similar thickness (approximately 3.5μm) whether the cells projected to V2 or MT (Table 2). The only clear difference between the two populations was a higher total dendritic length among MT-projecting cells (MT: 6,908μm, V2: 4,163μm; t-test, $p < 0.01$) (Table 3). This was particularly the case in layer 4B, where both cell types projecting to MT had significantly more dendritic length than those projecting to V2 (t-test, $p < 0.01$). It was clear simply by eye that V2-projecting cells had much sparser dendritic fields (Figures 2 and 3). Additionally, pyramidal neurons projecting to MT had apical dendrites that terminated significantly closer to the top of layer 1 than the apical dendrites of pyramids projecting to V2 (t-test, $p < 0.01$) (Table 2).

The positions of cells in layer 4B relative to the pattern of CO blobs in layer 2/3 were assessed for both pyramids and spiny stellates projecting to MT or V2. Since our sections were cut perpendicular to the cortical surface, we could not plot the locations of our cells relative to a complete two dimensional map of CO blobs. Instead, we measured the distance of each cell body to the closest two CO blobs on either side and computed a blob distance index (Table 2; Figure 4C) (see Experimental Procedures). A blob distance index of zero indicates a cell body directly underneath a blob center, whereas a blob distance index of one indicates a cell body within an interblob, equidistant from the blobs on either side. Given that our injections into V2 likely included all three CO stripe types, we expected our V2-projecting layer 4B cells to be located indiscriminately underneath both blobs and interblobs and this was indeed the case (blob distance index = 0.60) (Table 2; Figure 4C) (Sincich and Horton, 2002,2003). Previous studies regarding the MT-projecting population are much less clear, with some evidence for no bias (Shipp and Zeki, 1989;Sincich and Horton, 2003) and other evidence for patchiness biased to the blobs (Boyd and Casagrande, 1999). The overall population of MT-projecting cells which we labeled did not show a clear bias toward blobs or interblobs (blob distance index = 0.35). It is important to note that our total number of labeled cells was rather low and may have precluded us from observing a bias present in the population. However, when we analyzed the relationship of the individual cell types to the blob pattern, we were surprised to find that pyramidal cells were consistently located underneath blobs (Figures 2B and 4C). While spiny stellates showed no apparent bias to blobs or interblobs (blob distance index = 0.43), pyramidal cells showed a strong bias to the blobs (blob distance index = 0.21) (Table 2). Among MT-

projecting cells, pyramids were found significantly closer to blob centers than stellates (Mann-Whitney test, $p < 0.01$). Furthermore, MT-projecting pyramids were found significantly closer to blob centers than V2-projecting pyramids (Mann-Whitney test, $p < 0.001$). This result might explain much of the previous discrepancy in the literature and has interesting circuit implications for connectivity with M versus P pathways.

DISCUSSION

Our observations provide evidence for a highly specialized population of neurons projecting directly from V1 to MT, which are functionally dominated by the M pathway. These neurons are distinct from those projecting to V2, which integrate information from both the M and P pathways. The specialized functional roles of neurons projecting to MT versus V2 are implied by the anatomical specializations we observed, as schematized in Figure 5. We find that neurons projecting from V1 to MT are mostly spiny stellate cells, whereas those projecting to V2 are mainly pyramidal. Furthermore, the minority of MT projecting cells that do have a pyramidal morphology are located preferentially underneath CO blobs, whereas stellates projecting to MT and neurons of both cell types projecting to V2 do not show any apparent bias toward blobs or interblobs. Thus, all layer 4B neurons that project to MT restrict their dendrites to regions that receive strong input from the M-recipient layer 4Cα. Regardless of cell type, neurons projecting to MT are also much larger than those projecting to V2 and have more total dendritic length, particularly within layer 4B. Together, these observations imply that the MT projecting neurons are specialized for the rapid transmission of information carried by the M pathway, while slower computations involving mixed M and P inputs are mediated by V2-projecting neurons (Figure 5).

We found that neurons projecting from layer 4B of V1 to MT are a majority spiny stellate. These neurons likely convey M-dominated input to MT as stellates have been shown to receive input only from M-dominated layer 4Cα (Yabuta et al., 2001). It is particularly striking that stellates make up the majority cell type that projects to MT, since they are only a small minority of the neurons within layer 4B (Callaway and Wiser, 1996). It is important to note, however, that small numbers of pyramids project to MT as well. Since disynaptic input to MT has previously been shown to originate almost exclusively from M-dominated layer 4Cα (Nassi and Callaway, 2006), it is possible that the small numbers of pyramidal cells that project to MT receive input only from M-dominated layer 4Cα and are, therefore, distinct from the majority of pyramids in layer 4B that receive mixed M and P inputs. This suggestion is further supported by the preferential location of MT-projecting pyramids underneath blobs (see further below). In contrast to the population projecting to MT, we found pyramidal cells to be the majority cell type projecting to V2. These neurons likely convey mixed M and P inputs to V2 and possibly indirectly to MT (Yabuta et al., 2001; Nassi and Callaway, 2006). Taken together, these results suggest that the projection from V1 to MT is highly specialized and distinct from other V1 outputs.

Neurons projecting to MT could be distinguished from those projecting to V2 based on numerous parameters beyond cell type. Previous studies have reported that MT-projecting neurons are considerably larger than those projecting to V2 (Sincich and Horton, 2003). This was indeed the case, with the average neuron projecting to MT more than double the size of the average neuron projecting to V2. Importantly, this difference in cell body size could not be explained simply by stellates being larger than pyramids (Table 2), suggesting that even the pyramids projecting to MT are distinct from those projecting to V2. The larger cell body size of the MT-projecting cells is likely to correspond to a greater axon diameter, which would mediate relatively fast action potential conduction (Rockland, 1995).

Neurons projecting to MT were also located deeper within layer 4B, closer to the layer 4Cα border, than neurons projecting to V2. We believe that a more heterogeneous population of V2-projecting pyramidal cells scattered throughout the depth of layer 4B largely accounts for this difference; again, suggesting that the pyramids projecting to MT may be part of a specialized population distinct from pyramids projecting to V2 and other areas. Being located closer to layer 4Cα may allow MT-projecting neurons to receive more extensive input from M layers of the LGN or neurons in M-dominated layer 4Cα. Indeed, layer 4B neurons located more superficially within layer 4B consistently had less dendritic length extending into layer 4Cα (data not shown).

In analyzing the laminar distribution of dendrites for neurons of each type projecting to MT or V2, it was apparent that there existed considerable similarities. Regardless of cell type or projection target, all layer 4B neurons had the vast majority of their dendrites in layers 4B and 4Cα, with small amounts of dendrite consistently present in layer 4A as well. None of the neurons ever had dendrites extending below layer 4Cα and only pyramidal neurons had dendrites extending above layer 4A. There were, however, a few important differences between the populations projecting to MT or V2. The most striking difference was that MT-projecting neurons had much more total dendritic length than V2-projecting neurons, particularly in layer 4B. This may be an indication that neurons projecting to MT receive more extensive input from other neurons in layer 4B or layer 4Cα. It was also the case that pyramids projecting to MT had more dendritic length in layer 2/3 than pyramids projecting to V2, with the apical dendrites of the former terminating significantly closer to the top of layer 1. Pyramids projecting to V2 often had apical dendrites that terminated well below layer 1, whereas those projecting to MT typically had apical dendrites that extended to the pia. Direct thalamic input from K layers in the LGN as well as feedback connections from MT and other areas may be received via the apical dendrite of MT-projecting pyramids within layer 1 (Blasdel and Lund, 1983; Ding and Casagrande, 1997; Shipp and Zeki, 1989).

Interestingly, pyramids projecting to MT were found consistently underneath CO blobs. Previous studies in macaque monkey have not observed a blob bias among MT-projecting neurons (Shipp and Zeki, 1989; Sincich and Horton, 2003), likely due to the fact that the majority of these neurons are spiny stellates which were found indiscriminately underneath both blobs and interblobs in the present study. Only when analyzing MT-projecting pyramids separately from the total population of neurons did a blob bias become apparent among this cell type. Boyd and Casagrande (1999) reported a blob bias in bush baby and owl monkey which may be partly explained by the fact that pyramids constitute the majority of MT-projecting cells in these monkey species (Diamond et al., 1985; Shipp and Zeki, 1989). It may be that pyramids projecting to MT are preferentially located underneath CO blobs because, unlike interblobs, this is a location where apical dendrites are able to sample M input from layer 4Cα (Lachica et al., 1992; Yabuta and Callaway, 1998). This would be consistent with the fact that neurons projecting directly from V1 to MT have been shown previously to receive input almost exclusively from the M pathway (Nassi and Callaway, 2006). In contrast, pyramids projecting to the CO thick stripes in V2, which in turn project to MT, are preferentially located underneath CO interblobs (Sincich and Horton, 2002) where apical dendrites only have access to P input from layer 4Cβ (Lachica et al., 1992). This is consistent with the fact that neurons projecting from V1 to V2 have been shown previously to receive mixed input from both M and P pathways (Nassi and Callaway, 2006). We suggest that activity dependent developmental processes may underlie the selection of MT-projecting pyramids underneath the CO blobs due to the matching input pattern from the M pathway. MT-projecting pyramids underneath interblobs could receive P input, resulting in a mismatch between input and output. This mismatch could lead to the retraction of the apical dendrite (Koester and O'Leary, 1992; Callaway, 1998b). Alternatively, pyramids underneath interblobs might initially project to multiple cortical areas and then retract projections to MT (Barone et al., 1995). These results

serve as yet another indication that even the small numbers of pyramids that project to MT are specialized and distinct from those projecting to V2 and other areas.

Area MT receives its main ascending input from a highly specialized and distinct population of neurons in layer 4B of V1. This population of neurons allows M-dominated signals to be conducted quickly to MT despite the convergence of M and P pathways onto the majority of neurons within layer 4B. It is known that MT-projecting V1 neurons are highly direction selective (Movshon and Newsome, 1996), but more studies are necessary to fully characterize their response profiles. Neurons projecting from layer 4B of V1 to V2 receive convergent M and P inputs and likely relay different visual computations indirectly to MT. Future studies that can identify and record from each of the many input pathways to MT will be necessary to elucidate the functional contributions of each pathway to visual responses in MT and to the perception of motion and depth.

EXPERIMENTAL PROCEDURES

Surgical procedures

Four adult macaque monkeys were used, following procedures approved by the Salk Institute Animal Care and Use Committee. In addition, all procedures using rabies virus were conducted using biosafety level 2 precautions as described previously (Kelly and Strick, 2000).

A 1.5 tesla Siemens (Erlangen, Germany) Symphony magnetic resonance scanner (University of California, San Diego Hillcrest Medical Center/Tenet Magnetic Resonance Institute, San Diego, CA) was used to obtain a full coronal series of 1-mm-thick images for each monkey used for injections into MT (JNM2, JNM14). Resulting structural images were used to calculate stereotaxic coordinates for our injections along the posterior bank of the STS. For V2 injections, we simply targeted the opercular surface just posterior to the lip of the lunate sulcus.

MT was targeted in two monkeys, JNM2 (right hemisphere) and JNM14 (both hemispheres). MT injections were made using Hamilton syringes with a 30 gauge needle. In monkey JNM2 two penetrations spaced 1mm apart in the anterior-posterior plane were aimed at the posterior bank of the STS. Approximately 0.3μl of the SAD ΔG-EGFP rabies virus (see below, Rabies virus strain) was injected at each of four depths spaced 1mm apart. In monkey JNM14, two penetrations were made into the posterior STS of each hemisphere, and 0.3μl of virus was injected at five different depths similarly as in JNM2.

V2 was targeted in two monkeys, JNM8 (right hemisphere) and JNM12 (right hemisphere). V2 injections were made by using glass micropipettes (tip diameter, ~30 μm), and pressure was applied by a Picospritzer. In monkey JNM8, four penetrations were made along the opercular surface, perpendicular to the cortical surface, just posterior to the lip of the lunate sulcus. Penetrations were each separated by 10mm mediolaterally. Approximately 0.3μl of virus with 10% rhodamine dextran (10,000 MW; Molecular Probes, Carlsbad, CA) was injected at each of three depths spaced 0.5mm apart. In monkey JNM12 ten penetrations were made, each separated by 2mm mediolaterally. Approximately 0.3μl of virus (without rhodamine) was injected similarly as in JNM8.

Rabies virus strain

To retrogradely label neurons that project directly from V1 to MT or V2, we injected the SAD ΔG-EGFP rabies virus and allowed a survival time of 7 days (except for a 3 day survival time for JNM2). This strain of rabies virus was obtained from Dr. Karl-Klaus Conzelmann, Max Von Pettenkofer Institute (Munich, GR). Studies have shown that rabies virus infects at axon terminals and travels only in the retrograde direction (Kelly and Strick, 2000; Ugolini, 1995). The rabies virus used in our study is derived from the SAD B19 vaccine strain of the rabies

virus and has had its envelope glycoprotein gene replaced with the gene for GFP (Etessami et al., 2000). The glycoprotein of the rabies virus is essential for viral infection at axon terminals, so viral particles injected into the brain have glycoprotein on their membrane, infect cells at axon terminals, travel retrogradely within the cell, and express GFP. Importantly, though, new viral particles produced within the cell do not have glycoprotein on their membrane and are unable to infect further cells across synapses. The SAD ΔG-EGFP rabies virus has been shown to be a powerful monosynaptic retrograde tracer, expressing GFP at high levels up to 16 days post injection, with no evidence of cell lysis or virus spillage into the surrounding neuropil (Wickersham et al., 2007).

Histology

After 7 days survival time (except for a 3 day survival time for JNM2) the animals were killed by overdose with sodium pentobarbital and perfused with 4% paraformaldehyde (2% for JNM8), and their brains were removed. Sections were cut using a freezing microtome. In cases JNM2 and JNM14 sections were cut in two separate blocks. One block contained cortex including and posterior to the lunate sulcus (V1) and was cut parasagittally at 40μm (JNM2) or 60μm (JNM14). The other block contained cortex anterior to the lunate sulcus and was cut coronally at 40μm. In case JNM8 sections were also cut in two separate blocks. V2 cortex was dissected away from V1, flattened, and cut tangentially at 50μm. Remaining cortex was cut coronally at 60μm. In case JNM12 a single block was cut coronally at 60μm through V1 and V2.

First a series of every 12^{th} section was processed for both CO and GFP. We used this initially processed series to determine the extent of label in V1. Regions containing retrogradely labeled cells were processed in entirety. Each section was stained first for CO, followed by GFP immunostaining. Immunohistochemistry for GFP was performed by using the anti-GFP rabbit polyclonal antibody (Molecular Probes, Carlsbad, CA), the biotinylated goat anti-rabbit secondary antibody (Vector Laboratories, Burlingame, CA), and an ABC avidin-peroxidase kit (Vector Laboratories) and was revealed via a diaminobenzidine (DAB) reaction enhanced with nickel and cobalt (black reaction product).

For cases JNM2 and JNM14 a series of cortical sections that included the STS was processed for myelin, CO and GFP, or Nissl substance. Anatomical features of MT (Tootell et al., 1985; Van Essen et al., 1981), such as heavy and uniform myelination (particularly in deep layers), dark and patchy CO staining, greater cortical thickness, and relative position on the posterior bank of the STS, were used to verify that injections were confined to area MT (see Figures 1A–B). Tangential (JNM8) and coronal (JNM12) sections through V2 were processed for CO and GFP to visualize the V1/V2 border and to verify that injections were confined to V2.

In the MT injections our needle penetrations likely involved some white matter directly underneath cortex. Previous studies have shown that rabies virus uptake along cut peripheral axons is inefficient compared with uptake at axon terminals, and rabies uptake along cut central axons has not been demonstrated (Kelly and Strick, 2000; Ugolini, 1995). In addition, in two other monkeys we injected directly into the white matter, missing cortex altogether. These cases resulted in a complete absence of labeled cells anywhere in the surrounding cortex (data not shown), suggesting that uptake and retrograde GFP labeling with the SAD ΔG-EGFP rabies virus and a 7 day survival time can only occur via axon terminals in cortex. We found no evidence of white matter uptake in JNM2 or JNM14, with retrogradely labeled cells localized to layers 4B and 6 in V1, exactly what we would expect from an injection in cortical MT (Shipp and Zeki, 1989).

Data analysis

Retrogradely labeled cells within V1 were classified as pyramidal or spiny stellate only when a sufficient number of adjacent sections were available to determine the presence or absence of an apical dendrite extending above layer 3. Those cells that had an apical dendrite extending above layer 3 were classified as pyramidal, and those without such an apical dendrite were classified as spiny stellate. Labeled cells for which we could not conclusively determine the presence or absence of an apical dendrite were not included in the analysis. Dendritic reconstructions of labeled cells were carried out at 40x with Neurolucida software (MicroBrightField, Williston, VT). Reconstructions were subsequently analyzed using Matlab algorithms to calculate parameters such as dendritic length per cortical layer. Importantly, because cells extended through multiple adjacent sections, laminar borders were redrawn for each section and dendritic processes were assigned to a layer based on the laminar borders drawn for that same section.

Cell body sizes (area and perimeter) were determined by outlining the cell body at 20x. Cell bodies that were partially cut-off were not included in this analysis. Apical dendrite thickness was measured with 40x magnification at the first clear inflection points along the dendrite as it extended away from the cell body. Laminar depth was calculated by plotting the point where the main descending axon leaves the cell body. The distance between this point and the layer 4B/4A border was divided by the total thickness of layer 4B, resulting in a laminar depth index. An index of one indicates a cell body at the bottom of layer 4B and an index of zero indicates a cell body at the top of layer 4B. The apical dendritic laminar depth index was calculated by plotting the point at which the apical dendrite terminates. The distance between this point and the top of layer 1 was divided by the total thickness of layers 1–3. An index of zero indicates an apical dendrite that terminates at the top of layer 1.

The point where the main descending axon leaves the cell body was also plotted to calculate a CO blob distance index. Locations of CO blob centers were plotted for the two blobs to the immediate left and right of the cell body. The lateral distance (parallel to cortical layers) of the CO blob closest to the cell body was divided by the distance to the other blob, resulting in a blob distance index ranging from zero to one. An index of one indicates a cell body in an interblob and equidistant between two adjacent blob centers, while an index of zero indicates a cell body directly underneath a blob center. The angle of the plane of section relative to vertical was calculated by taking the sine of the tissue thickness divided by the radial blood vessel length. When this angle was greater than 25°, CO blob centers were plotted in an adjacent section (aligned with the blood vessel pattern from original section) in which layer 3 was estimated to be directly vertical from the cell body.

Acknowledgments

We are grateful for support from the National Institutes of Health. We thank Dr. Karl-Klaus Conzelmann for providing the SAD ΔG-EGFP rabies virus, Cecelia Kemper for technical assistance with structural MRIs, and Mauricio De La Parra for assistance with animal care and surgical procedures. We also thank Dr. Ian Wickersham for sharing expertise with the rabies virus and Karine von Bochmann for assistance with computer reconstructions of labeled neurons.

References

Barone P, Dehay C, Berland M, Bullier J, Kennedy H. Developmental remodeling of primate visual cortical pathways. Cereb Cortex 1995;5:22–38. [PubMed: 7719128]

Blasdel GG, Lund JS. Termination of afferent axons in macaque striate cortex. J Neurosci 1983;3:1389–1413. [PubMed: 6864254]

Boyd JD, Casagrande VA. Relationships between cytochrome oxidase (CO) blobs in primate primary visual cortex (V1) and the distribution of neurons projecting to the middle temporal area (MT). J Comp Neurol 1999;409:573–591. [PubMed: 10376741]

Burkhalter A, Felleman DJ, Newsome WT, Van Essen DC. Anatomical and physiological asymmetries related to visual areas V3 and VP in macaque extrastriate cortex. Vision Res 1986;26:63–80. [PubMed: 3716214]

Callaway EM. Local circuits in primary visual cortex of the macaque monkey. Annu Rev Neurosci 1998a; 21:47–74. [PubMed: 9530491]

Callaway EM. Prenatal development of layer-specific local circuits in primary visual cortex of the macaque monkey. J Neurosci 1998b;18:1505–1527. [PubMed: 9454858]

Callaway EM, Wiser AK. Contributions of individual layer 2–5 spiny neurons to local circuits in macaque primary visual cortex. Vis Neurosci 1996;13:907–922. [PubMed: 8903033]

Dacey DM. Parallel pathways for spectral coding in primate retina. Annu Rev Neurosci 2000;23:743–775. [PubMed: 10845080]

Desimone, R.; Ungerleider, LG. Neural mechanisms of visual processing in monkeys. In: Boller, F.; Grafman, J., editors. Handbook of Neuropsychology. Amsterdam: Elsevier; 1989. p. 267-299.

DeYoe EA, Van Essen DC. Concurrent processing streams in monkey visual cortex. Trends Neurosci 1988;11:219–226. [PubMed: 2471327]

Diamond IT, Conley M, Itoh K, Fitzpatrick D. Laminar organization of geniculocortical projections in Galago senegalensis and Aotus trivirgatus. J Comp Neurol 1985;242:584–610. [PubMed: 2418082]

Ding Y, Casagrande VA. The distribution and morphology of LGN K pathway axons within the layers and CO blobs of owl monkey V1. Vis Neurosci 1997;14:691–704. [PubMed: 9278998]

Elston GN, Rosa MG. The occipitoparietal pathway of the macaque monkey: comparison of pyramidal cell morphology in layer III of functionally related cortical visual areas. Cereb Cortex 1997;7:432–452. [PubMed: 9261573]

Etessami R, Conzelmann KK, Fadai-Ghotbi B, Natelson B, Tsiang H, Ceccaldi PE. Spread and pathogenic characteristics of a G-deficient rabies virus recombinant: an in vitro and in vivo study. J Gen Virol 2000;81:2147–2153. [PubMed: 10950970]

Hendrickson AE, Wilson JR, Ogren MP. The neuroanatomical organization of pathways between the dorsal lateral geniculate nucleus and visual cortex in Old World and New World primates. J Comp Neurol 1978;182:123–136. [PubMed: 100530]

Hendry SH, Reid RC. The koniocellular pathway in primate vision. Annu Rev Neurosci 2000;23:127–153. [PubMed: 10845061]

Hendry SH, Yoshioka T. A neurochemically distinct third channel in the macaque dorsal lateral geniculate nucleus. Science 1994;264:575–577. [PubMed: 8160015]

Kelly RM, Strick PL. Rabies as a transneuronal tracer of circuits in the central nervous system. J Neurosci Methods 2000;103:63–71. [PubMed: 11074096]

Koester SE, O'Leary DD. Functional classes of cortical projection neurons develop dendritic distinctions by class-specific sculpting of an early common pattern. J Neurosci 1992;12:1382–1393. [PubMed: 1556599]

Lachica EA, Beck PD, Casagrande VA. Parallel pathways in macaque monkey striate cortex: anatomically defined columns in layer III. Proc Natl Acad Sci U S A 1992;89:3566–3570. [PubMed: 1314392]

Livingstone M, Hubel D. Segregation of form, color, movement, and depth: anatomy, physiology, and perception. Science 1988;240:740–749. [PubMed: 3283936]

Livingstone MS, Hubel DH. Connections between layer 4B of area 17 and the thick cytochrome oxidase stripes of area 18 in the squirrel monkey. J Neurosci 1987;7:3371–3377. [PubMed: 2824713]

Maunsell JH, van Essen DC. The connections of the middle temporal visual area (MT) and their relationship to a cortical hierarchy in the macaque monkey. J Neurosci 1983;3:2563–2586. [PubMed: 6655500]

Merigan WH, Maunsell JH. How parallel are the primate visual pathways? Annu Rev Neurosci 1993;16:369–402. [PubMed: 8460898]

Michael CR. Retinal afferent arborization patterns, dendritic field orientations, and the segregation of function in the lateral geniculate nucleus of the monkey. Proc Natl Acad Sci U S A 1988;85:4914–4918. [PubMed: 3387448]

Movshon JA, Newsome WT. Visual response properties of striate cortical neurons projecting to area MT in macaque monkeys. J Neurosci 1996;16:7733–7741. [PubMed: 8922429]

Nassi JJ, Callaway EM. Multiple circuits relaying primate parallel visual pathways to the middle temporal area. J Neurosci 2006;26:12789–12798. [PubMed: 17151282]

Rockland KS. Morphology of individual axons projecting from area V2 to MT in the macaque. J Comp Neurol 1995;355:15–26. [PubMed: 7636009]

Shipp S, Zeki S. The Organization of Connections between Areas V5 and V1 in Macaque Monkey Visual Cortex. Eur J Neurosci 1989;1:309–332. [PubMed: 12106142]

Sincich LC, Horton JC. Divided by cytochrome oxidase: a map of the projections from V1 to V2 in macaques. Science 2002;295:1734–1737. [PubMed: 11872845]

Sincich LC, Horton JC. Independent projection streams from macaque striate cortex to the second visual area and middle temporal area. J Neurosci 2003;23:5684–5692. [PubMed: 12843271]

Sincich LC, Jocson CM, Horton JC. Neurons in v1 patch columns project to v2 thin stripes. Cereb Cortex 2007;17:935–941. [PubMed: 16740582]

Tigges J, Tigges M, Anschel S, Cross NA, Letbetter WD, McBride RL. Areal and laminar distribution of neurons interconnecting the central visual cortical areas 17, 18, 19, and MT in squirrel monkey (Saimiri). J Comp Neurol 1981;202:539–560. [PubMed: 7298914]

Tootell RB, Hamilton SL, Silverman MS. Topography of cytochrome oxidase activity in owl monkey cortex. J Neurosci 1985;5:2786–2800. [PubMed: 2995611]

Ugolini G. Specificity of rabies virus as a transneuronal tracer of motor networks: transfer from hypoglossal motoneurons to connected second-order and higher order central nervous system cell groups. J Comp Neurol 1995;356:457–480. [PubMed: 7642806]

Van Essen DC, Maunsell JH, Bixby JL. The middle temporal visual area in the macaque: myeloarchitecture, connections, functional properties and topographic organization. J Comp Neurol 1981;199:293–326. [PubMed: 7263951]

vogt Weisenhorn DM, Illing RB, Spatz WB. Morphology and connections of neurons in area 17 projecting to the extrastriate areas MT and 19DM and to the superior colliculus in the monkey Callithrix jacchus. J Comp Neurol 1995;362:233–255. [PubMed: 8576436]

Wickersham IR, Finke S, Conzelmann KK, Callaway EM. Retrograde neuronal tracing with a deletion-mutant rabies virus. Nat Methods 2007;4:47–49. [PubMed: 17179932]

Xiao Y, Felleman DJ. Projections from primary visual cortex to cytochrome oxidase thin stripes and interstripes of macaque visual area 2. Proc Natl Acad Sci U S A 2004;101:7147–7151. [PubMed: 15118090]

Yabuta NH, Callaway EM. Functional streams and local connections of layer 4C neurons in primary visual cortex of the macaque monkey. J Neurosci 1998;18:9489–9499. [PubMed: 9801386]

Yabuta NH, Sawatari A, Callaway EM. Two functional channels from primary visual cortex to dorsal visual cortical areas. Science 2001;292:297–300. [PubMed: 11303106]

Yoshioka T, Levitt JB, Lund JS. Independence and merger of thalamocortical channels within macaque monkey primary visual cortex: anatomy of interlaminar projections. Vis Neurosci 1994;11:467–489. [PubMed: 8038123]

Zeki S, Shipp S. The functional logic of cortical connections. Nature 1988;335:311–317. [PubMed: 3047584]

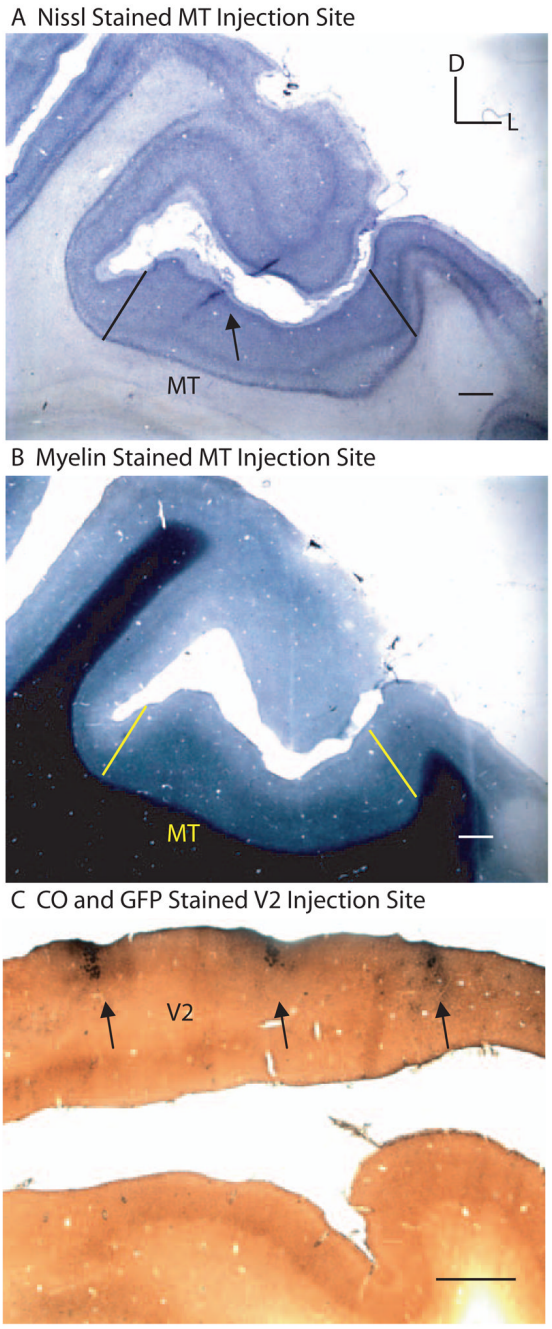

Figure 1. Rabies virus injection sites in MT or V2. (A)
A single coronally cut cortical section stained for Nissl showing the needle track location (black arrow) within the STS. Black lines denote the approximate lateral and medial borders of MT as determined by myelin. **(B)** A coronally cut cortical section, adjacent to that in **(A)**, stained for myelin. Yellow lines denote the approximate lateral and medial borders of the uniformly dense myelination pattern typical of MT. D, dorsal; L, lateral. Scale bars in **(A)** and **(B)** equal 100μm. **(C)** A single coronally cut cortical section stained for cytochrome oxidase (CO; brown) and GFP (black) showing the locations of rabies injected regions (black arrows) along the opercular surface in V2. Scale bar equals 1mm.

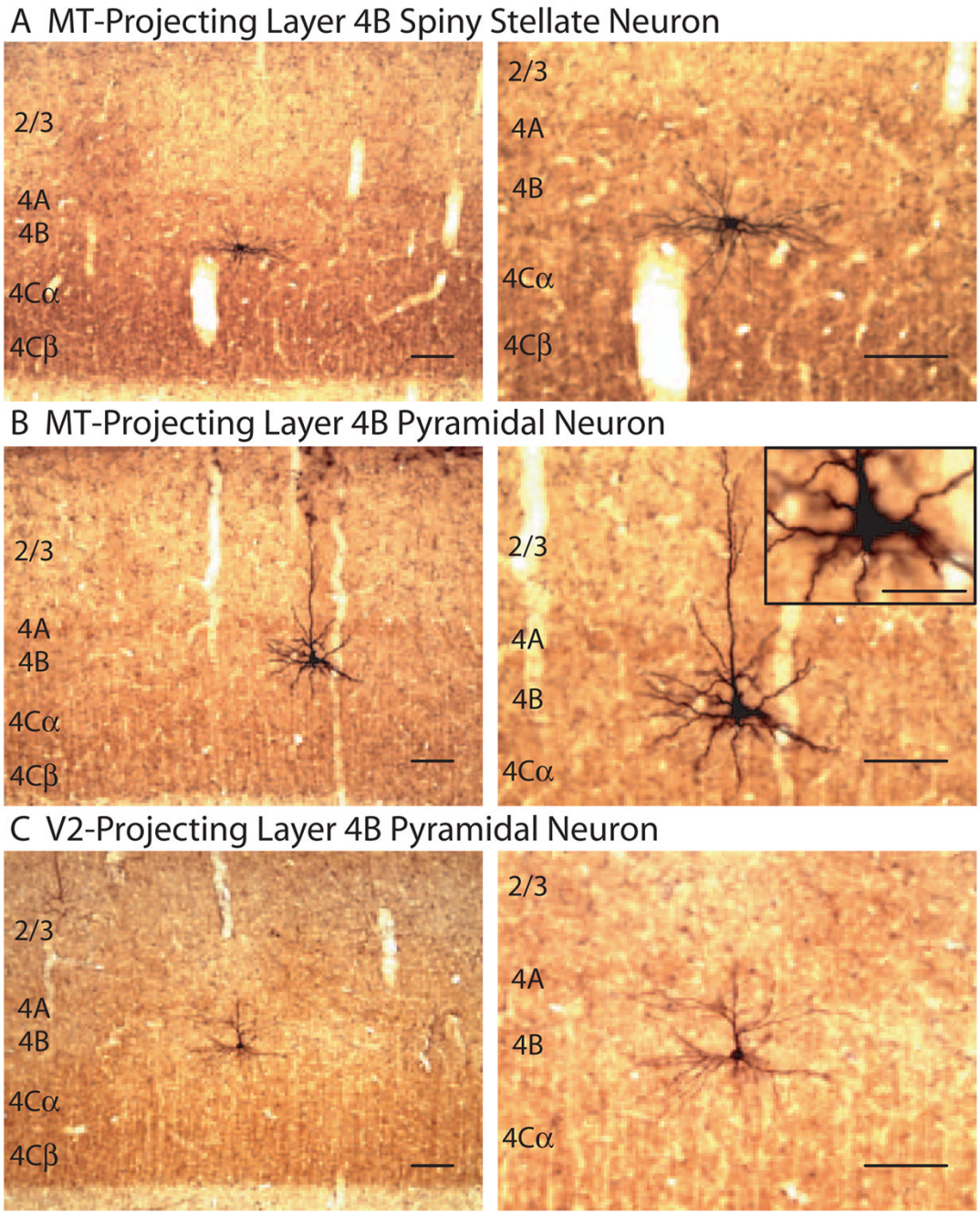

Figure 2. Retrogradely labeled neurons in layer 4B of V1 after injections in MT or V2.

(A and B) Parasagittal sections stained for CO and GFP showing a spiny stellate neuron **(A)** or pyramidal neuron **(B)** in layer 4B of V1 retrogradely labeled from MT. **(C)** A coronal section stained for CO and GFP showing a pyramidal neuron in layer 4B of V1 retrogradely labeled from V2. Low (left) and high (right) magnification images are shown with cortical layers indicated. A single higher magnification image is shown in the inset of **(B)**. Scale bars in **(A) and (C)** equal 100 μm. Scale bar in inset of **(B)** equals 50μm.

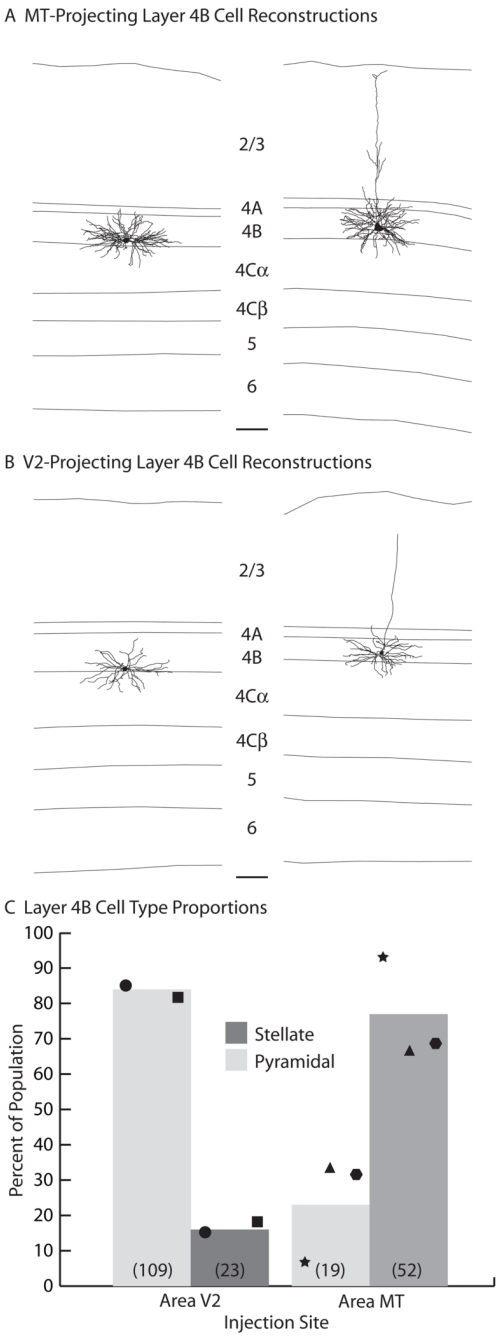

Figure 3. Cell types projecting from layer 4B of V1 to MT or V2
(A and **B)**
Computer-assisted dendritic reconstructions of spiny stellate (left) and pyramidal (right) neurons projecting to MT **(A)** or V2 **(B)**. Layers are indicated. Scale bars equal 100μm. **(C)** The average percentages of spiny stellate (dark gray) and pyramidal (light gray) neurons projecting to MT or V2. Cases JNM2 (star), JNM14L (triangle), and JNM14R (hexagon) for MT, and JNM8 (circle) and JNM12 (square) for V2 are shown. Total numbers of each cell type are indicated in parentheses.

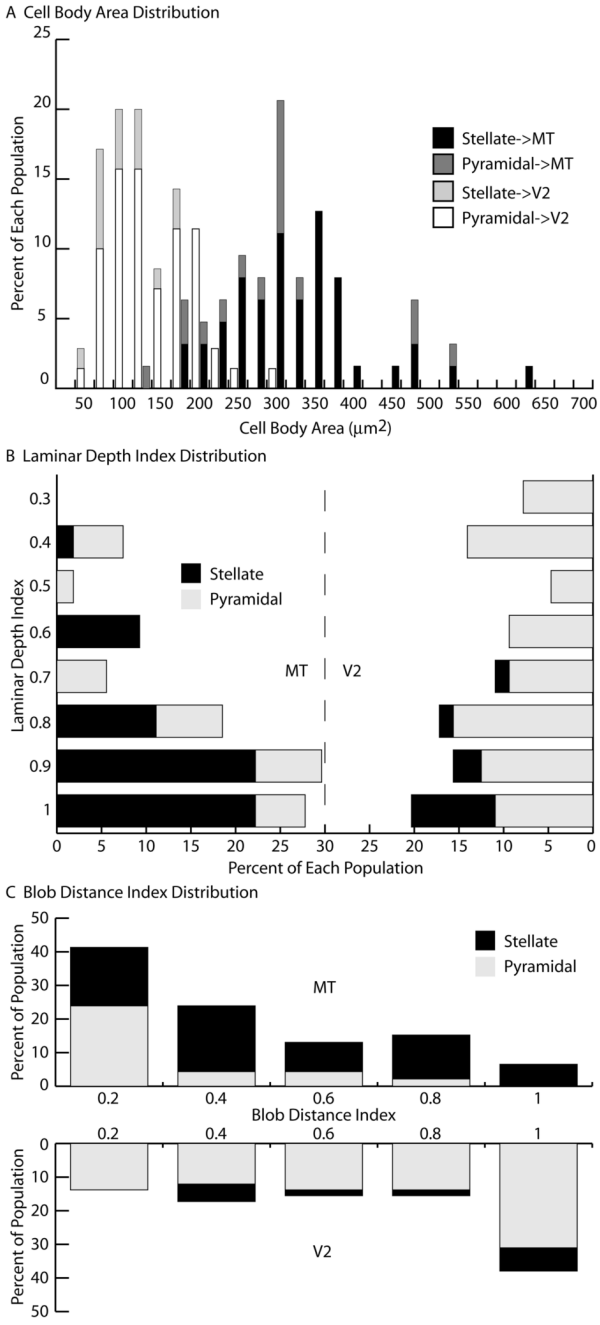

Figure 4. Anatomical differences between V1 neurons projecting to MT or V2. (A) Percentages of layer 4B spiny stellate (black) and pyramidal (dark gray) neurons projecting to MT or spiny stellate (light gray) and pyramidal (white) neurons projecting to V2 according to their cell body area. **(B)** Percentages of layer 4B spiny stellate (black) and pyramidal (gray) neurons projecting to MT (left) or V2 (right) according to their laminar depth index. An index value of 1 indicates a neuron at the bottom of layer 4B and an index value of 0 indicates a neuron at the top of layer 4B. **(C)** Percentages of layer 4B spiny stellate (black) and pyramidal (gray) neurons projecting to MT (top) or V2 (bottom) according to their blob distance index. An index value of 1 indicates a neuron centered in an interblob equidistant from the two closest blobs and an index value of 0 indicates a neuron centered directly underneath a blob.

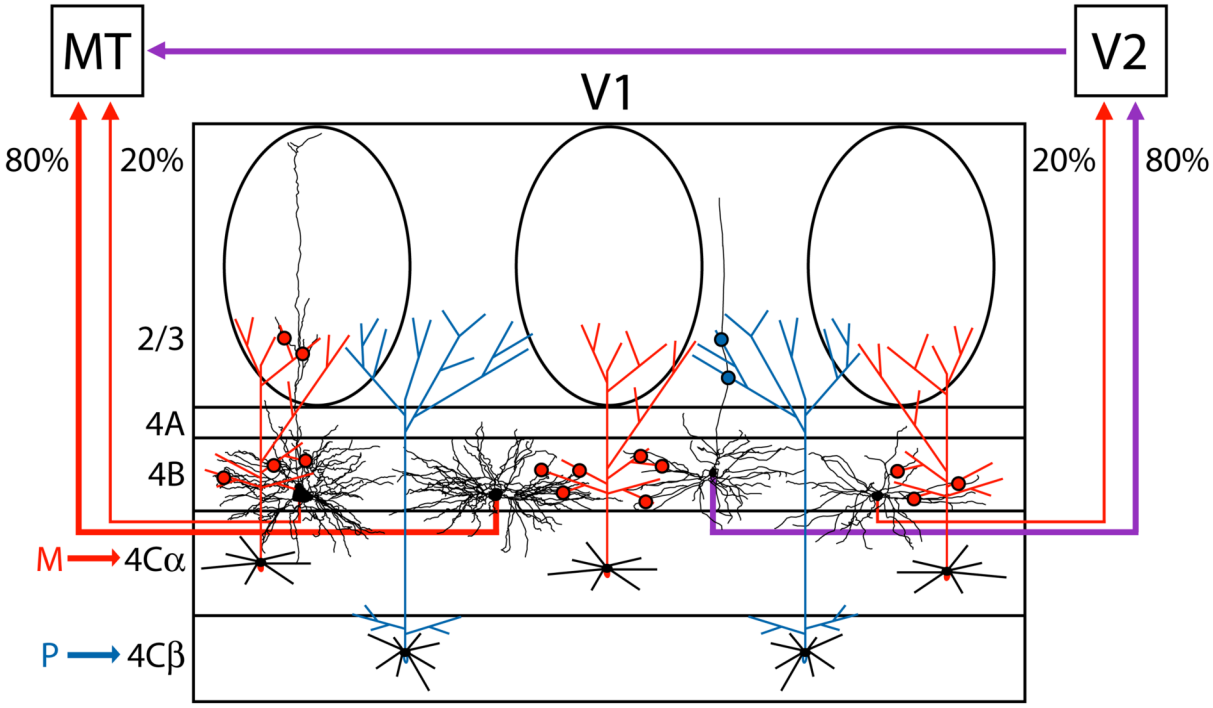

Figure 5. Specialized circuits from V1 to V2 and area MT

Schematic of circuits carrying M and P inputs to MT or V2, through layers 4C and 4B of V1. Both spiny stellates (80%, *middle-left*) and pyramids (20%, *far left*) that project from V1 to MT restrict their dendrites to zones receiving M input (red arrow) via layer 4Cα neurons (red axons). These zones include layer 4B and the overlying CO blobs of layer 2/3. The projection from layer 4B of V1 to MT is, therefore, dominated by the M pathway (red arrows). In contrast, the majority of layer 4B neurons that project to V2 are pyramids (80%, *middle-right*) located underneath both blobs and interblobs. These neurons integrate both P input (blue arrow) via layer 4Cβ neurons (blue axons) and M input (red arrow) via layer 4Cα neurons (red axons) to provide a combined M and P projection to V2 and indirectly to MT (purple arrows). The minority spiny stellates (20%, *far right*) that project to V2 provide a weak M input (red arrow). Dendrites are shown in black. The locations of putative synaptic contacts from axons of layer 4Cα neurons onto dendrites of layer 4B neurons are schematized by red dots and those from layer 4Cβ neurons by blue dots. Layer 4B neurons are computer reconstructions taken from Figure 3. Layers are indicated.

Table 1

Cell type proportions.

Injection Target	Case	Number of Stellates	Number of Pyramids	Number of Cells Total	Proportion Stellate	Average Proportion
MT	JNM2	14	1	15	0.93	0.76
	JNM14R	9	4	13	0.69	
	JNM14L	29	14	43	0.67	
	Combined	52	19	71	0.73	———
V2	JNM8	3	17	20	0.15	0.17
	JNM12	20	92	112	0.18	
	Combined	23	109	132	0.17	———

Table 2

Cell anatomical measurements

Mean values are in bold. Values in square brackets to the right of the mean indicate numbers of cells. Values in parentheses below the mean indicate the standard errors.

Injection Target	Cell Type	Cell Body Area (μm^2)	Cell Body Perimeter(μm)	Laminar Depth Index	Blob Distance Index	Apical Dendrite Thickness (μm)	Tufted Apical Dendrite Prop	Apical Dendrite Laminar Depth Index
MT	Stellate	**335.84** [46] (12.97)	**67.87** [46] (1.31)	**0.81** [36] (0.03)	**0.43** [30] (0.05)	———	———	———
	Pyramidal	**309.60** [17] (26.82)	**66.44** [17] (3.03)	**0.71** [18] (0.05)	**0.21** [16] (0.04)	**3.46** [18] (0.25)	**0.22** [18] (0.15)	**0.10** [18] (0.02)
	Combined	**328.76** [63] (11.89)	**67.49** [63] (1.25)	**0.78** [54] (0.02)	**0.35** [46] (0.04)	———	———	———
V2	Stellate	**121.23** [15] (10.03)	**41.83** [15] (2.05)	**0.90** [10] (0.03)	**0.63** [9] (0.08)	———	———	———
	Pyramidal	**153.22** [55] (6.98)	**46.80** [55] (1.09)	**0.63** [54] (0.03)	**0.60** [49] (0.05)	**3.50** [31] (0.15)	**0.22** [36] (0.12)	**0.18** [36] (0.02)
	Combined	**146.36** [70] (6.07)	**45.73** [70] (0.98)	**0.68**[64] (0.03)	**0.60** [58] (0.04)	———	———	———

Table 3

Dendritic length by layer

Mean values are in bold and indicate either the length of dendrites found in a layer (μm) or the proportion of total dendritic length found in a layer (prop). Values in parentheses below the means indicate the standard errors. Values in parentheses to the right of the cell type names indicate the numbers of cells reconstructed.

		Average Dendritic Lenth										
Injection Target	**Cell Type**	**Layer 2/3**		**Layer 4A**		**Layer 4B**		**Layer 4C α**		**Layer 4C β–6**		**Total**
		μm	**prop**	**μm**	**prop**	**μm**	**prop**	**μm**	**prop**	**μm**	**prop**	**μm**
MT	Stellate (5)	**0** (0)	**0** (0)	**51.8** (17.8)	**0.01** (0)	**5,373.6** (677.7)	**0.79** (0.05)	**1,414.1** (173.8)	**0.21** (0.05)	**0** (0)	**0** (0)	**6,839.5** (530.7)
	Pyramidal (5)	**564.5** (95.2)	**0.08** (0.02)	**160.5** (43.5)	**0.02** (0.01)	**5,081.3** (265.1)	**0.73** (0.01)	**1,169.6** (286.3)	**0.17** (0.03)	**0** (0)	**0** (0)	**6,975.8** (430.2)
	Combined (10)	**282.2** (104.2)	**0.04** (0.02)	**106.2** (28.6)	**0.02** (0)	**5,227.5** (346.5)	**0.75** (0.03)	**1,291.8** (163.1)	**0.19** (0.03)	**0** (0)	**0** (0)	**6,907.7** (322.9)
V2	Stellate (3)	**0** (0)	**0** (0)	**4.1** (4.1)	**0.01** (0)	***1,997.7*** (194.7)	**0.68** (0.01)	**867.6** (382.2)	**0.29** (0.02)	**0** (0)	**0** (0)	**2,869.3** (191.7)
	Pyramidal (5)	**384.6** (57.0)	**0.08** (0.01)	**182.7** (91.3)	**0.04** (0.01)	**3,248.9** (439.6)	**0.66** (0.05)	**1,122.5** (274.9)	**0.23** (0.07)	**0** (0)	**0** (0)	**4,938.7** (474.2)
	Combined (8)	**240.4** (78.2)	**0.05** (0.01)	**115.7** (63.6)	**0.02** (0.01)	**2,779.7** (354.2)	**0.66** (0.03)	**1,026.9** (211.7)	**0.26** (0.04)	**0** (0)	**0** (0)	**4,162.7** (477.1)